The PPARβ/delta-induced mesenchymal stromal cell secretome has cytoprotective effects via ANGPTL4 in a pre-clinical model of acute lung inflammation

Courteney Tunstead[1], Molly Dunlop[1], Sinéad Ryan[1], Evelina Volkova[1], Evangeline Johnston[1], Sabrina Batah[2], Claudia C. Dos Santos[2], Bairbre McNicholas [3,4], Claire Masterson[3,4], John G. Laffey[3,4] & Karen English[1,5,*]

[1]*Cellular Immunology Lab, Department of Biology, Maynooth University, Maynooth, Co. Kildare, Ireland.*

[2] *Keenan Research Centre for Biomedical Research, St. Michael's Hospital, Toronto, Canada.*

[3]*Anesthesia and Intensive Care Medicine, School of Medicine, College of Medicine Nursing and Health Sciences, University of Galway, Galway, Ireland.*

[4]*Anesthesia and Intensive Care Medicine, Galway University Hospitals, Saolta University Hospitals Groups, Galway, Ireland.*

[5]*Kathleen Lonsdale Institute for Human Health Research, Maynooth University, Maynooth, Co. Kildare, Ireland.*

[*]*Corresponding author*

Corresponding author information

Prof. Karen English

karen.english@mu.ie

Keywords: MSC, ARDS, Lung reapir, ANGPTL4, PPARβ/δ

ABSTRACT

Rationale: Human bone marrow-derived mesenchymal stromal cells (hBM-MSCs) are known to exert immunomodulatory and pro-reparative effects *in vivo*. This makes hBM-MSCs an enticing therapeutic candidate for inflammatory diseases, such as acute respiratory distress syndrome (ARDS). The ARDS microenvironment is complex and contains an abundance of free fatty acids (FFAs); which are known to differentially impact MSC functionality. PPARβ/**δ** is a ubiquitously expressed nuclear receptor that is activated in response to FFA-binding. PPARβ/**δ** has been shown to impact the therapeutic efficacy of mouse MSCs. **Objective:** This study sought to investigate the impact of PPARβ/**δ**-modulation on human MSC functionality *in vitro* and *in vivo.* **Methods:** hBM-MSCs were exposed to a synthetic PPARβ/**δ** agonist/antagonist in the presence or absence of ARDS patient serum and the immunomodulatory and pro-reparative capacity of the MSC secretome was investigated using *in vitro* assays and a pre-clinical model of LPS-induced acute lung inflammation (ALI). **Results:** Our results highlighted enhanced pro-reparative capacity of PPARβ/**δ**-agonised hBM-MSCs secretome in CALU-3 lung epithelial cells, mediated by MSC derived angiopoietin-like 4 (ANGPTL4). PPARβ/**δ**-induced ANGPTL4-high MSC secretome facilitated enhanced endothelial barrier integrity in the lungs of ALI mice. Therapeutic effects of PPARβ/**δ**-agonised hBM-MSCs secretome were further enhanced by licensing MSCs with human ARDS patient serum. ARDS-licensed PPARβ/**δ**-induced ANGPTL4-high MSC secretome had reduced clinical score and weight loss. The role ANGPL4 in these protective effects was confirmed using an anti-ANGPTL4 antibody. **Conclusion:** These findings conclude that the MSC secretome therapeutic effects can be enhanced both *in vitro* and *in vivo* through licensing strategies that upregulate the angiogenic factor ANGPTL4.

53

54 **INTRODUCTION**

55

56 Cell therapy, particularly mesenchymal stromal cell (MSC) therapy, has long been thought of
57 as a therapeutic candidate in the treatment of many inflammatory diseases. This is largely due
58 to their immunomodulatory and cytoprotective capacity [1]. One of the conditions that MSCs
59 have been considered for is acute respiratory distress syndrome (ARDS); an inflammatory,
60 degenerative condition of the lung [2, 3]. MSCs have been trialled and tested for ARDS over
61 the last 20 years, but clinical trials have shown poor outcomes; with ~60% non-responders [4-
62 6]. The environment into which MSCs are administered can alter their functional capacity [7-
63 9]. There is limited understanding of how the ARDS microenvironment may impact MSCs.
64 The complex ARDS microenvironment contains inflammatory-mediators, microorganisms,
65 and free fatty acids (FFAs). These components have all been shown to impact MSC therapeutic
66 capacity in various ways [10, 11]. Our previous work highlighted the differential effect of the
67 hypo-inflammatory vs hyper-inflammatory ARDS microenvironment on MSC therapeutic
68 efficacy with a clear correlation between high levels of inflammation, and enhanced MSC-
69 driven repair [12]. We, and others, have also demonstrated that FFAs can influence MSC-
70 induced immunosuppressive effects [13, 14]. In this study, we wanted to investigate the
71 influence of FFAs present in the ARDS patient microenvironment, and the impact they have
72 on hBM-MSCs in a pre-clinical model of acute lung inflammation (ALI).

73 The peroxisome proliferator-activated receptor-beta/delta (PPARβ/**δ**) is a ubiquitously-
74 expressed nuclear receptor, present on all nucleated cells including hBM-MSCs, that is
75 activated in response to FFA exposure [15, 16]. In recent years, PPARβ/**δ** has been shown to
76 impact MSC therapeutic efficacy [17-27]. Interestingly, there are differential findings with
77 some studies showing that deficiency of PPARβ/**δ** enhances MSC immunosuppressive effects

[21, 22], while other studies demonstrate similar immunosuppressive effects mediated by both naive and PPARβ/**δ**-deficient mouse MSCs [24]. Studies have shown enhanced immunomodulatory capacity of T-cells by PPARβ/**δ**-inhibited mouse MSCs [21, 22]. Differentially, PPARβ/**δ** antagonism of MSCs impaired MSC therapeutic effects while priming of mouse MSCs with a PPARβ/**δ** agonist enhanced MSC cardioprotective effects *in vivo* [25]. Moreover, cardioprotective effects of MSCs were shown to be PPARβ/**δ**-dependent as the therapeutic effect was lost when PPARβ/**δ**-deficient mouse MSCs were administered [24]. These findings suggest that natural ligands of PPARβ/**δ** may have positive or detrimental effects on MSC efficacy *in vivo*. Due to the abundance of FFAs in the ARDS microenvironment, we sought to investigate the impact of PPARβ/**δ** (via synthetic agonism or antagonism) on the human BM-MSC secretome; and report the impact this had on immunomodulation and cytoprotection, in a model of ALI.

105

106 **MATERIALS AND METHODS**

107

108 **hBM-MSC cell culture**

109 Human bone marrow-derived MSCs (hBM-MSCs; RoosterBio™) were cultured in Dulbecco's
110 Modified Eagle Medium (DMEM) containing 10% foetal bovine serum (FBS) and 1%
111 *Penicillin streptomycin* (cDMEM). The cells were cultured for 5 days at 37°C + 5% CO_2. All
112 experiments are a representation of three independent MSC donors.

113

114 **Generation and concentration of MSC-CM**

115 hBM-MSCs (passage 2-5) from three independent donors were seeded at a density of $1x10^5$
116 per well in a 6-well plate in 1ml of cDMEM and allowed to adhere. Once adhered, the cells
117 were stimulated with 1µM of PPARβ/**δ** agonist (GW0742, Tocris™) or antagonist (GSK3787,
118 Tocris™), as previously described [12]. 24hrs-post stimulation, the cells were washed with
119 PBS, and the media was replaced with serum-free DMEM. This was left for a further 24hrs to
120 allow for the generation of MSC-CM. When including ARDS serum-exposure, the
121 agonist/antagonist were washed from the cells, and 20% ARDS serum was added for 24hrs.
122 This was then washed away, and serum-free DMEM was added for a further 24hrs to allow for
123 the generation of MSC-CM. All MSC-CM was harvested and stored at -20°C for future
124 experiments. MSC-CM was then concentrated, as required, as previously described [12].

125

126 **Gene & Protein expression**

127 For gene expression, RNA was isolated and normalised to 100 ng/µl. cDNA was generated
128 using the QuantBio™ cDNA Synthesis kit (as per manufacturer's instructions). Real-time
129 reverse transcription polymerase chain reaction (RT-PCR) was run using PerfeCta SYBR

130 Green FastMix (QuantBio™) and pre-made Sigma™ primers (supplementary table 1). Relative
131 expression was quantified in relation to *hprt* by calculating the 2-ΔΔCT values. For protein
132 expression, 96-well half-area ELISA plates (COSTAR™) were coated as per manufacturers
133 guidelines (human ANGPTL4 and VEGF (R&D™)) and run as previously described [12].
134

135 **Sequencing & metabolomic analysis**

136 hBM-MSCs were seeded at a density of $1x10^5$ in a 6-well plate and allowed to adhere. Once
137 attached, the cells were exposed to 1μM of PPARβ/**δ** agonist (GW0742, Tocris™) or
138 antagonist (GSK3787, Tocris™) and incubated for 6hrs. This dose was chosen based on
139 previous research from our group [19]. The cells were harvested in TRIzol for RNA isolation.
140 RNA was isolated through a series of chloroform and isopropanol extractions. RNA
141 concentration and purity was assessed using Nanodrop 2000 (Thermo Fisher Scientific) and
142 samples were sent to Novogene™ for sequencing (GEO accession no.: GSE281162). Processed
143 RNA sequencing datasets, provided by Novogene™, were then used to identify differentially
144 expressed genes (DEGs) of interest. Volcano plots highlighting the most significantly enriched
145 genes were generated using Flourish™ software. Data was also collected from publicly
146 available RNA sequencing (GEO accession no.: GSE185263) and metabolomic datasets (Study
147 ID: ST000042; doi: 10.21228/M8SG64). Normalised values were taken from both studies and
148 data was plotted using GraphPad Prism™ (version 10) software.
149

150 **Scratch Assay**

151 CALU-3 lung epithelial cells (cultured as previously described) [12] were seeded at a density
152 of $5x10^5$ in a 6-well plate. Once 80% confluent, a single vertical scratch was made down the
153 centre of the well using a p200 tip. The cells were then washed with PBS to remove debris, and
154 MSC-CM was added for a period of 6 - 48hrs. The cells were then fixed with 10% formalin,

155 before allowing to dry. Once dry, the cells were stained with crystal violet, allowed to dry, and
156 imaged. To avoid bias, a marker was used to denote an area in the upper, central and lower
157 regions of each scratch and images were taken from these points (supplementary figure 1).
158 Mitomycin C (Sigma™) was added to assess the impact of proliferation at a concentration of
159 5 µg/ml for 2hrs prior to the scratch assay.
160

161 **Scratch Assay Analysis**

162 Three images, taken at each of the three marked points, were taken per well; for each of the
163 three independent MSC donors (i.e. 3 images per well x 3 MSC donors = 9 images per group).
164 Fiji/ImageJ™ software was then used to divide each picture into four distinct quadrants in an
165 unbiased manner (Analyse -> Tools -> Grid -> set area per point to 44444 inches squared).
166 This grid includes the addition of 4 horizontal lines imputed on the image. Using the straight-
167 line feature in Fiji/ImageJ™ software, four measurements were then taken per picture at each
168 of the horizontal lines. This provided 4 measurements per picture, at unbiased points, to get a
169 clear depiction of each percentage wound closure. The average wound closure per donor was
170 calculated, and divided by the baseline scratch value, to get the final percentage wound closure
171 (supplementary figure 1).
172

173 **Study cohorts and ethical approval for patient samples**

174 Ethical approval was obtained from Galway University Medical Ethics Committee and
175 Maynooth University Ethics Committee. All participants provided full consent.
176

177 **ARDS serum extraction**

178 Serum samples from both male and female patients, aged 40-80 years old, were taken from
179 patients with SARS-CoV-2-induced ARDS, from the patient pools we previously
180 characterised and described [12].

181

182 **ANGPTL4 Neutralisation**

183 MSC-CM was exposed to 5 µg/ml of ANGPTL4 neutralising antibody (Cell Sciences™), or 5
184 µg/ml IgG2aκ isotype control (Rockland Immunochemicals™). This was incubated at room
185 temperature for 1hr prior to use. This concentration was utilised as per manufacturer guidelines
186 for our study.

187

188 **ALI mouse model**

189 Male and female C57BL6/J mice (Charles River), aged 8+ weeks were exposed to 2mg/kg of
190 endotoxin (Sigma, 0001:B4 Serotype), or PBS control administered intratracheally (IT) with a
191 total of 42 animals with sample size determined based on similar studies in the published
192 literature. For IT administration, mice were placed in an isoflurane chamber with a steady flow
193 of both isoflurane and oxygen for 30-45 seconds, depending on the weight of the mouse. Mice
194 were then placed on the IT stand, and a nose cone of isoflurane was used in increments
195 throughout the administration to ensure sufficient anaesthesia. Mice were randomized to
196 groups according to cage mate sex and ID sequence. A single animal represents the
197 experimental unit; and within each cage, there were mice receiving different treatments to
198 account for potential confounders with numbers per group outlined in each figure legend. There
199 was no specific inclusion or exclusion criteria used for this study; any animals not accounted
200 for across all groups were due to required euthanasia prior to experimental end-point and
201 limitation on the amount of ARDS patient serum available. Animals were identified using a
202 numerical ID for the purpose of this study. Although information regarding groupings and

203 treatments was available to the lead researchers, the numerical IDs were used for data harvest
204 and data analysis to prevent bias in result interpretation. MSC-CM was prepared as described
205 in the methods section. 500µl of PPARβ/**δ**-modulated MSC-CM, i.e. the equivalent of what
206 would be produced from $5x10^4$ (low dose) of hBM-MSCs, was then concentrated to a volume
207 of 30µl and administered intranasally (IN) 4hrs post-endotoxin challenge under light isoflurane
208 anaesthesia for 15-30 seconds. An Evan's Blue permeability assay was carried out by
209 administration of an intravenous (IV) tail vein injection of sterile-filtered Evan's Blue Dye
210 (10%) 1hr prior to harvesting. The mice were sacrificed using an intraperitoneal (IP) injection
211 of pentobarbital. Absorbance readings were taken to assess the total Evan's Blue (620nm and
212 740nm) in bronchoalveolar lavage fluid (BALF) blood and whole lungs. Measurements taken
213 from the mice included (a) pro-inflammatory cytokines screening of the BALF, (b) Evan's
214 Blue permeability absorbances/images, and (c) clinical scoring (based on HPRA-approved
215 scoring methodology) and weight loss. Statistical analysis was performed using GraphPad
216 Prism 10 software and statistical tests used have been highlighted in the figure legends of each
217 figure. The work has been reported in line with the ARRIVE guidelines 2.0.
218
219 **Statistical Analysis**
220 Power calculations were performed to guide sample size, and data were analyzed using
221 GraphPad Prism 10 software. One-way ANOVA, or where appropriate a Two-way ANOVA
222 followed by the post hoc Tukey's multiple comparison test, was used to assess significance.
223 For figure 2C, a t-test was carried out to identify significance in DEGs. All data are presented
224 as mean ± SEM and the n numbers are outlined in each figure legend.
225
226
227

228 **RESULTS**

229

230 **The $MSC_{PPARβ/δ(+)}$ secretome enhances pro-reparative capacity in CALU-3 lung epithelial**

231 **cells via migration and proliferation *in vitro***

232 A scratch assay in CALU-3 cells was used to investigate the impact of PPARβ/**δ** agonism (+)

233 or antagonism (-) on MSC conditioned medium (MSC-CM) capacity to promote wound healing

234 *in vitro* (figure 1A). Our data highlighted a significant increase in wound closure in both MSC-

235 CM_{Naive} and MSC-$CM_{PPARβ/δ(+)}$ groups (figure 1B, C). Interestingly, MSC-$CM_{PPARβ/δ(-)}$

236 promoted wound healing when compared to control medium but did not significantly enhance

237 CALU-3 wound closure. While there was no statistical difference between MSC-CM_{Naive} and

238 MSC-$CM_{PPARβ/δ(-)}$ (figure 1B), the percentage wound closure in the MSC-$CM_{PPARβ/δ(-)}$ group

239 was less than in the MSC-CM_{Naive} group. There is a possibility that PPARβ/**δ** antagonism could

240 lead to the production of inhibitory factors in the conditioned medium, however, our RNA-Seq

241 data set did not identify any known inhibitory factors (see figure 2, table 2). It is known that

242 wound closure can involve proliferation and or migration [28, 29], thus this experiment was

243 repeated using Mitomycin C; a known proliferation inhibitor [30]. While the addition of

244 Mitomycin C significantly reduced wound closure in the MSC-$CM_{PPARβ/δ(+)}$ group at the 48hr

245 time point, the percentage wound healing in the presence of Mitomycin C remained higher than

246 the medium control group suggesting that both proliferation and migration may have a

247 combination effect (figure 1D). Interestingly, significantly more wound repair was observed in

248 the MSC-$CM_{PPARβ/δ(+)}$ group compared to the MSC-CM_{Naive} group at 48hrs, while the MSC-

249 $CM_{PPARβ/δ(-)}$ group did not inhibit or enhance would healing (figure 1D). *TOP2A is* a gene

250 largely indicative of cell proliferation [31] and has previously been used as an indicator for cell

251 proliferation in wound healing. Gene expression analysis of *TOP2A* in CALU-3 cells

252 highlighted a significant difference between the MSC-$CM_{PPARβ/δ(+)}$ and MSC-$CM_{PPARβ/δ(-)}$

253 groups, with the MSC-CM$_{PPARβ/δ(+)}$ group having significantly more proliferative capacity than
254 the MSC-CM$_{PPARβ/δ(-)}$ group (figure 1E). Importantly, Mitoymcin C significantly reduced
255 *TOP2A* expression in the MSC-CM$_{Naive}$ and MSC-CM$_{PPARβ/δ(-)}$ groups (figure 1E).
256
257 **Analysis of MSC$_{PPARβ/δ(+)}$ RNA sequencing highlighted upregulation of ANGPTL4**
258 To try to identify the potential mechanisms associated with enhanced wound healing capacity
259 in MSC$_{PPARβ/δ(+)}$, RNA sequencing (Novogene™; GEO accession no.: GSE281162) was
260 performed on MSC$_{PPARβ/δ(+)}$, MSC$_{PPARβ/δ(-)}$ and MSC$_{Naive}$ (figure 2A). The data highlighted a
261 variety of differentially expressed genes (DEGs) between the three groups. The DEGs numbers
262 were visualised using a Venn diagram (figure 2B), showing 170 DEGs specific to the MSC$_{Naive}$
263 group, 128 specific to the MSC$_{PPARβ/δ(+)}$ group, and 189 specific to the MSC$_{PPARβ/δ(-)}$ group.
264 Volcano plot visualisation highlighted several of the most significantly altered DEGs in each
265 group (figure 2C). The MSC$_{PPARβ/δ(+)}$ group had a significant enrichment of genes such as
266 *PLIN2, ANGPTL4, FAM156A, CPT1A, CAT, NADK2, TMED6,* and *LDHAL6B.* This group
267 also showed significant downregulation in genes such as *MAGED4* and *FAM157B* (table 1).
268 The MSC$_{PPARβ/δ(-)}$ group had a significant enrichment of genes such as *IKBKGP1, SNRPGP2,*
269 *LINC01159, MIR3648-1, RARRES1, MALAT1* and *RNF217-AS1.* This group also showed
270 significant downregulation in genes such as *RGPD5, PFN1P3, MIR3936HG, U2AF1* and
271 *TSNAXIP1* (table 2). Fragments per kilobase of exon per million mapped fragments (FPKMs)
272 of two known PPARβ/**δ** target genes (angiopoietin like protein 4 (ANGPTL4) and pyruvate
273 dehydrogenase kinase 4 (PDK4)) were plotted to confirm the data was as expected (figure 2D,
274 E), and this was confirmed by qRT-PCR (figure 2F, G).
275
276 **MSC-associated genes/proteins are unaffected by PPARβ/δ agonism or antagonism;**
277 **except ANGPTL4**

278 Given the functional enhancement of MSC-CM$_{PPARβ/δ(+)}$ promotion of wound healing observed
279 in figure 1, the production of known cytoprotective factors released by MSCs were assessed.
280 While MSC$_{Naive}$ produced ANGPTL4, VEGF and MIF, MSC$_{PPARβ/δ(+)}$ only produced
281 significantly higher levels of ANGPTL4 (figure 3A-C). This aligns with the RNA-sequencing
282 data as *ANGPTL4* was the only cytoprotective factor differentially expressed in MSC$_{PPARβ/δ(+)}$.
283 Along with this, PPARβ/**δ** agonism/antagonism did not affect expression of typical MSC-
284 associated immunomodulatory factors such as *PTGS2, IL-6, IDO, PTGES* or *TGFβ (figure 3D-*
285 *H).*
286
287 **The secretome from MSC-CM$_{PPARβ/δ(+)}$ enhances wound healing in CALU-3 lung**
288 **epithelial cells in an ANGPTL4-dependent manner**
289 Other studies have highlighted the role of a PPARβ/**δ** agonist [18], and ANGPTL4 in
290 promoting repair in other tissues [29, 32]. It has also been shown that ANGPTL4 can play a
291 significant role in proliferation and migration [28]. To determine if the increased levels of
292 ANGPTL4 present in MSC-CM$_{PPARβ/δ(+)}$ played a role in the enhanced pro-reparative capacity,
293 we used an anti-ANGPTL4 neutralising-antibody to eliminate the functional capacity of
294 ANGPTL4 in the MSC-CM (figure 4A). Importantly, ANGPTL4-neutralisation but not the
295 isotype control antibody, abrogated the enhanced wound closure observed in the MSC-
296 CM$_{PPARβ/δ(+)}$ group (figure 4B-C). Addition of the ANGPTL4 neutralising antibody interfered
297 with ANGPTL4 protein levels as quantified by ELISA (figure 4D).
298
299 **Ligands and co-activators of PPARβ/δ are increased, while co-repressors of PPARβ/δ are**
300 **decreased, in ARDS patients**
301 Thus far, our data has shown that PPARβ/**δ** agonism leads to enhanced cytoprotective effects
302 of MSC-CM. Previously, it was deduced that MSC-CM derived from ARDS-serum licensed

303 MSCs has superior therapeutic effects in a pre-clinical model of ALI [12]. To ensure
304 translational relevance of our findings from this study in human conditions such as ARDS, a
305 publicly available metabolomics dataset (Study ID: ST000042; doi: 10.21228/M8SG64) was
306 mined. From this metabolomics dataset we identified that PPARβ/**δ** ligands are more prevalent
307 in ARDS. Higher levels of linoleate, palmitoleic acid and arachidonate were present in the
308 bronchoalveolar lavage fluid (BALF) from ARDS patients, in comparison to healthy controls
309 (figure 5A). Using a publicly available RNA sequencing dataset (GEO accession no.:
310 GSE185263), it was shown that several PPARβ/**δ**-associated co-activators that were increased
311 in the blood of ARDS patients when compared to Non-ARDS controls (figure 5B). This
312 included a significant increase in *NCOA1* and *NCOA3,* a trend toward increased *PPARGC1A*
313 and *NCOA2,* and no difference in *CREBBP* (figure 5C-G). Along with this, several PPARβ/**δ**-
314 associated co-repressors were decreased in the blood of the same ARDS patients (figure 5B).
315 This included a significant reduction in *SIRT1, NCOR1* and *NCOR2* (figure 5H-J). Given that
316 *ANGPTL4* was significantly upregulated in response to PPARβ/**δ** agonism in our own
317 sequencing dataset (figure 2), levels of ANGPTL4 were further assessed upon MSC-exposure
318 to ARDS patient serum. In comparison to the PPARβ/**δ** agonist, exposure of MSCs to ARDS
319 patient serum significantly increased MSC secretion of ANGPTL4. Addition of both the
320 PPARβ/**δ** agonist and ARDS patient serum further enhanced MSC production of ANGPTL4
321 (figure 5K). Interestingly, addition of the PPARβ/**δ** antagonist could not block the ARDS
322 serum induction of ANGPTL4 secretion by MSCs. This is largely down to PPARβ/**δ** having
323 multiple binding-sites [33], whereby both agonists and antagonists can bind simultaneously;
324 with agonism out-competing antagonism (supplementary figure 2).
325
326 **MSC-CM$_{PPARβ/δ(+)}$ provides enhanced lung endothelial barrier function in ALI**

327 Next, we investigated the protective effects of MSC-CM$_{PPARβ/δ(+)}$ in a preclinical model of LPS
328 induced-ALI. First we set out to determine the number of MSCs that could provide a
329 therapeutic effect in a mouse model of ALI, comparing two different doses of MSCs.
330 Administration of high dose MSCs ($1x10^5$) led to significant decrease in TNFα, IL-1β and IL-
331 6 in the BALF of ALI mice, while low dose MSCs (5×10^4) could only decrease TNFα and
332 led to increased IL-6 in the BALF (supplementary figure 3). Following this, MSC-CM that was
333 generated from the equivalent of the low dose was used; with the idea that using a low dose
334 would allow us to detect any enhanced therapeutic efficacy following PPARβ/**δ** agonism or
335 antagonism. This showed that MSC-CM$_{PPARβ/δ(+)}$ but not MSC-CM$_{PPARβ/δ(-)}$ significantly
336 improved the therapeutic efficacy of the non-efficacious dose of MSC-CM. Lungs of mice that
337 received MSC-CM$_{PPARβ/δ(+)}$ exhibited enhanced vascular and epithelial barrier function
338 measured using Evans Blue dye administration (figure 6A, B). Although modest, this result
339 was statistically powered. This effect was somewhat impacted by pre-exposing the MSC-CM
340 to anti-ANGPTL4 neutralising antibody, but this was not significantly different from the MSC-
341 CM$_{PPARβ/δ(+)}$ group (figure 6A, B). Indeed MSC-CM contains other growth factors and soluble
342 mediators that may also play a role in promoting lung repair and we cannot rule out the
343 possibility that other factors may contribute the protective effects observed. MSC-CM$_{PPARβ/δ(+)}$
344 did not significantly reduce the level of TNFα or IL-6 in the BALF of LPS-exposed mice
345 (figure 6C-D). Administration of MSC-CM$_{PPARβ/δ(+)}$ did not decrease weight loss or clinical
346 score in LPS-exposed mice (figure 6E-F).
347
348
349 **ARDS-licensed MSC-CM$_{PPARβ/δ(+)}$ provide protection in ALI in an ANGPTL4 dependent**
350 **manner**

351 Given our findings that MSC-CM$_{PPARβ/δ(+)}$ could enhance vascular and epithelial barrier
352 function but could not decrease BALF pro-inflammatory cytokines or reduce weight loss and
353 clinical score, we sought to investigate if we could increase the efficacy of MSC-CM.
354 Interestingly exposure to ARDS patient serum, along with PPARβ/**δ** agonism, allowed for a
355 10-fold increased induction of ANGPTL4 in MSC-CM compared to PPARβ/**δ** agonist alone
356 (figure 5K). Other proteins examined including IL-6, IL-8, VEGF, IL-1β and MIF
357 (supplementary figure 4) were not increased in MSCs that had been exposed to ARDS patient
358 serum, along with PPARβ/**δ** agonism. We hypothesised that ARDS-licensed MSC-
359 CM$_{PPARβ/δ(+)}$ would provide greater protection in ALI. In this case, the combination of ARDS
360 serum and PPARβ/**δ** agonism led to enhanced therapeutic effects with reduction in TNFα and
361 IL-6 in the BALF (figure 7A-B). Importantly, anti-ANGPTL4 reduced the anti-inflammatory
362 effects mediated by the ARDS-licensed MSC-CM$_{PPARβ/δ(+)}$ (figure 7A-B).
363 In line with this, there was a significant reduction in percentage weight-loss in mice exposed
364 to ARDS-licensed MSC-CM$_{PPARβ/δ(+)}$ (figure 7C), and again, this effect was abrogated in the
365 presence of the anti-ANGPTL4-neutralising antibody (figure 7C). Interestingly, we saw a non-
366 significant trend toward a reduced clinical score in mice exposed to ARDS-licensed MSC-
367 CM$_{PPARβ/δ(+)}$ (figure 7D). ANGPTL4-neutralisation appeared to abrogate this effect (figure 7D).
368
369
370
371 **DISCUSSION**
372
373 There are two primary functions of MSCs in the context of cell therapy: immunomodulation
374 and promotion of repair [1]. It is known that the environment can largely dictate MSC response
375 [7, 11, 34]. In the context of ARDS, the complex patient microenvironment; containing

376 inflammatory-agents, microorganisms and FFAs, can notably impact MSC functionality [10,
377 35]. We previously highlighted that higher levels of inflammation in the ARDS patient
378 microenvironment can promote VEGF-driven repair [12]. Abreu *et al.* (2020) investigated the
379 detrimental impact of fungal toxins present in the lung on MSC viability and showed a drastic
380 increase in MSC cell-death in response to this microenvironmental element [7]. However, there
381 has been little focus on how the FFAs in the ARDS patient microenvironment may impact
382 MSCs [36]. FFAs are known natural ligands of PPARβ/**δ** [37-39]. Importantly, studies have
383 already shown that modulation of this receptor can alter MSC functionality [17, 20, 21, 23, 25].
384 Given this, we wanted to investigate the functional impact of PPARβ/**δ**-modulation on both
385 primary functions of MSCs; immunomodulation and/or pro-reparative capacity.

386 In the case of pro-reparative capacity, PPARβ/**δ**-activation enhanced MSC-CM
387 mediated wound repair in CALU-3 lung epithelial cells (figure 1B, C). A time-lapse
388 experiment, using a mitomycin C proliferation inhibitor, highlighted that this was likely a
389 combination effect of both migration and proliferation (figure 1D, E). In the context of
390 promoting tissue repair, MSC secretion of VEGF [40-43], and HGF [44, 45] among other
391 factors have been shown to play key roles. However, PPARβ/**δ**-activation did not lead to
392 differential expression of VEGF or HGF. Interestingly, ANGPTL4 was significantly increased
393 in PPARβ/**δ** agonised MSCs. It has already been shown in several studies that ANGPTL4 can
394 promote both migration and proliferation in endothelial cells [28, 29]. Ziveri *et al.* (2024)
395 recently published a comprehensive study comparing the role of ANGPTL4 cytoprotection in
396 skin and brain endothelial cells. ANGPTL4 in the brain endothelium protects against bacterial
397 sepsis, and addition of ANGPTL4 to the skin endothelium, which naturally has lower levels of
398 ANGPTL4, leads to protection against bacterial sepsis [27]. ANGPTL4 has also been shown
399 to improve cardiac function in a mouse model of myocardial infarction [46]. Moreover, human
400 MSCs produced increased levels of ANGPTL4 following co-culture with THP-1 macrophages

401 *in vitro* [46]. Based on the identification of increased expression of ANGPTL4 in PPARβ/**δ**
402 agonised MSCs in our RNA-seq data set, we used an anti-ANGPTL4 antibody to neutralise the
403 ANGPTL4 in the MSC secretome, before addition to the CALU-3 lung epithelial cells (figure
404 4B-D). This abrogated the enhanced wound closure we had originally observed in our MSC-
405 $CM_{PPARβ/δ(+)}$ group.

406 We identified increased levels of PPARβ/**δ** ligands and co-activators in ARDS patient
407 samples using publicly available datasets. Exposure to ARDS patient serum significantly
408 increased ANGPTL4 levels produced by MSCs. A combination of MSC exposure to ARDS
409 patient serum and a PPARβ/**δ** agonist further increased ANGPTL4 levels. This proves that
410 MSCs are receptive to FFAs/other PPARβ/**δ** ligands presents in the ARDS microenvironment.
411 This aligns to our previous study where we identified that human BM-MSCs produce
412 significantly increased levels of ANGPTL4 in response to the FFA palmitate [14].

413 To enhance the clinical relevance of our findings, we showed that MSC-$CM_{PPARβ/δ(+)}$
414 mediated protective effects in ALI significantly enhancing vascular and epithelial barrier
415 integrity *in vivo*. Indeed, other studies have demonstrated that MSC-CM can mediate
416 therapeutic effects *in vivo* in ALI models [47] including our own study [12]. Our previous study
417 showed that MSC-CM generated from the equivalent of $5x10^4$ MSCs was ineffective in the
418 treatment of ALI; but licensing $5x10^4$ MSCs with ARDS patient serum enhanced the
419 therapeutic efficacy [12]. Using this approach of MSC-CM generated from the non-efficacious
420 dose of $5x10^4$ MSCs, we investigated the potential for enhanced efficacy of MSC-CM
421 generated from $5x10^4$ MSCs that had been exposed to a PPARβ/**δ** agonist or antagonist. MSC-
422 $CM_{PPARβ/δ(+)}$ provided enhanced efficacy over and above MSC-$CM_{PPARβ/δ(-)}$ in a pre-clinical
423 model of ALI. While there was a significant difference in the capacity for MSC-$CM_{PPARβ/δ(+)}$
424 in enhancing barrier function, addition of the ANGPTL4-neutralising antibody failed to
425 significantly impair this effect. This may be associated with growth factors or mediators other

426 than ANGPTL4 present in the MSC-CM$_{PPARβ/δ(+)}$ that may be contributing to the protective
427 effects observed. Our study demonstrated that ARDS patient serum induced significantly
428 higher levels of ANGPTL4 in MSC-CM and that combination with a PPARβ/**δ** agonist further
429 increased it. While MSC-CM$_{PPARβ/δ(+)}$ did not significantly reduce proinflammatory cytokines
430 in the BALF, ARDS licensed MSC-CM$_{PPARβ/δ(+)}$ reduced TNFα and IL-6 in the BALF of ALI
431 mice. By combining the PPARβ/**δ** agonist and licensing with ARDS patient serum, we created
432 MSC-CM with greater immunosuppressive capacity when compared to MSC-CM$_{PPARβ/δ(+)}$
433 alone. This is likely associated with the ~10-fold increase in ANGPTL4 levels when using the
434 combined licensing approach as addition of the ANGPTL4 neutralising antibody reversed the
435 trend. The limitation to these findings is the small numbers of mice (n=3/group) included in
436 the study for the ARDS licensed MSC-CM$_{PPARβ/δ(+)}$ treatment group. This was associated with
437 a limited volume of ARDS patient serum available for the study.

438 Here we provide novel findings to demonstrate that human BM-MSCs are responsive
439 to FFAs (ligands that bind PPARβ/**δ**) present in the ARDS patient environment, leading to
440 significantly increased levels of ANGPTL4 production. For the first time, we show that MSC-
441 derived ANGPTL4 plays an important role in promoting epithelial repair and enhancing
442 vascular barrier integrity. As most published studies have focused on mouse MSCs, we have
443 also addressed the gap in the knowledge of how PPARβ/**δ** influences human BM-MSC
444 cytoprotective and immunosuppressive functions. In this study, focusing on ALI, we did not
445 detect any significant positive or negative effects associated with PPARβ/**δ** antagonism in
446 hBM-MSCs. However, PPARβ/**δ** agonism enhanced MSC-CM promotion of wound healing
447 *in vitro* and vascular and barrier integrity *in vivo*. Furthermore, the combined approach of
448 PPARβ/**δ** agonism and licensing with ARDS patient serum produced an MSC-CM that could
449 suppress pro-inflammatory cytokines in the BALF of ALI mice.
450

451 **Declarations**

452 This manuscript has been uploaded to Bioxriv as a pre-print.

453

454 **Author Contributions**

455 C.T. performed research, data analysis, and study design and wrote the manuscript. M.D., S.R.,
456 E.V., E.J., S.B. and C.M. provided expertise and or performed research and data analysis.
457 B.McN and J.G.L. provided patient samples and data for the study. C.C.D.S and J.G.L.
458 contributed to study design. K.E. designed and supervised the study and wrote the manuscript.
459 All authors approved the final manuscript.

460

461 **Funding**

462 This research was supported by a Science Foundation Ireland Award to K.E. and J.G.L
463 (20/FFP-A/8948). This publication has emanated from research supported in part by the
464 National Irish Covid Biobank, through which our patient samples were collected and stored.

465

466 **Competing interests**

467 The authors declare no competing interests.

468

469 **Ethical Approval and HPRA Compliance**

470 Ethical approval was granted by the Maynooth University research ethics committee (BRESC-
471 2022-2453953) granted 17th February 2022 under the title: Cell based therapeutics for acute
472 respiratory distress syndrome for the animal studies and by Galway University Hospitals
473 Research Ethics Committee and by the Maynooth University research ethics committee
474 (BSRESC-2022-2482563) granted 14th October 2022 under the title: Human serum

475 Sepsis/ARDS MSC. HPRA approval was granted under the project authorisation(s)
476 AE19124/P031/P037.
477 RoosterBio (company where the human BM-MSCs were purchased) has confirmed that there
478 was initial ethical approval for collection of human cells, and that the donors had signed
479 informed consent. RoosterBio state "RoosterBio sources commercially available in vitro
480 research only human bone marrow aspirate from qualified donors. All human bone marrow
481 aspirate collections are from healthy adult consented donors. Collection protocols and the
482 donor-informed consent document are approved by an Institutional Review Board (IRB)"
483

484 **Use of AI**

485 The authors declare that they have not used AI-generated work in this manuscript.
486

487 **Data availability statement**

488 The RNA-sequencing dataset generated in our lab is available through GEO accession no.:
489 GSE281162. The other publicly available data sets are available online as outlined in the
490 Methods section. The remaining data supporting the findings of this study are available upon
491 request from the corresponding author.
492

493 **Acknowledgements**

494 The authors are grateful to the ARDS patients who donated the samples used in this study. We
495 would like to thank Rebecca Kerrigan, Deirdre Daly and Gillian O'Meara for the outstanding
496 care of the animals used in this study. Schematic figures contained in this manuscript have been
497 created using biorender.com.
498
499

500 **Table 1: DEG functions in $MSC_{PPARβ/δ(+)}$ group.**

Gene name	Up/Down	Involved in
plin2	Up	Lipid metabolism
angptl4	Up	Lipid metabolism and angiogenesis
fam156A	Up	Enables protein binding
cpt1A	Up	Lipid metabolism
cat	Up	Protection against oxidative stress
nadk2	Up	Protection against oxidative stress
tmed6	Up	Trafficking and transport
ldhal6B	Up	Lactate metabolism
maged4	Down	Cell cycle regulation
fam157B	Down	Non-coding

501

502 **Table 2: DEG functions in $MSC_{PPARβ/δ(-)}$ group.**

503

Gene name	Up/Down	Involved in
ikbkgp1	Up	NFκB signalling
snrpgp2	Up	RNA processing
linc01159	Up	Cell differentiation
mir3648-1	Up	Cell differentiation
rarres1	Up	Cell differentiation & retinoid signalling
malat1	Up	Cell differentiation
rnf217-as1	Up	Cell differentiation

rgpd5	Down	GTPase regulation
pfn1p3	Down	Cell motility/migration
mir3936hg	Down	Proliferation and apoptosis
u2af1	Down	ROS production/oxidative stress
tsnaxip1	Down	RNA processing and transport

504

505 **REFERENCES**

506

507 1. Faircloth, T.U., et al., *Vascular endothelial growth factor secretion and*
508 *immunosuppression are distinct potency mechanisms of human bone marrow*
509 *mesenchymal stromal cells.* Stem Cells, 2024. **42**(8): p. 736-751.
510 2. Matthay, M.A. and G.A. Zimmerman, *Acute lung injury and the acute respiratory*
511 *distress syndrome: four decades of inquiry into pathogenesis and rational*
512 *management.* Am J Respir Cell Mol Biol, 2005. **33**(4): p. 319-27.
513 3. Yang, X., et al., *Clinical course and outcomes of critically ill patients with SARS-*
514 *CoV-2 pneumonia in Wuhan, China: a single-centered, retrospective, observational*
515 *study.* Lancet Respir Med, 2020. **8**(5): p. 475-481.
516 4. Kaffash Farkhad, N., et al., *Mesenchymal stromal cell therapy for COVID-19-induced*
517 *ARDS patients: a successful phase 1, control-placebo group, clinical trial.* Stem Cell
518 Res Ther, 2022. **13**(1): p. 283.
519 5. Bowdish, M.E., et al., *A Randomized Trial of Mesenchymal Stromal Cells for*
520 *Moderate to Severe Acute Respiratory Distress Syndrome from COVID-19.* Am J
521 Respir Crit Care Med, 2023. **207**(3): p. 261-270.

522 6. Gorman, E., et al., *Repair of acute respiratory distress syndrome by stromal cell*
523 *administration (REALIST) trial: A phase 1 trial.* EClinicalMedicine, 2021. **41**: p.
524 101167.
525 7. Abreu, S.C., et al., *Differential effects of the cystic fibrosis lung inflammatory*
526 *environment on mesenchymal stromal cells.* Am J Physiol Lung Cell Mol Physiol,
527 2020. **319**(6): p. L908-L925.
528 8. Hawthorne, I.J., et al., *Human macrophage migration inhibitory factor potentiates*
529 *mesenchymal stromal cell efficacy in a clinically relevant model of allergic asthma.*
530 Mol Ther, 2023. **31**(11): p. 3243-3258.
531 9. Corbett, J.M., et al., *Cyclosporine A and IFNγ licencing enhances human*
532 *mesenchymal stromal cell potency in a humanised mouse model of acute graft versus*
533 *host disease.* Stem Cell Res Ther, 2021. **12**(1): p. 238.
534 10. Dunbar, H., et al., *The Inflammatory Lung Microenvironment; a Key Mediator in*
535 *MSC Licensing.* Cells, 2021. **10**(11).
536 11. Rolandsson Enes, S., et al., *Healthy versus inflamed lung environments differentially*
537 *affect mesenchymal stromal cells,* Eur Respir J, 2021. **58**(4).

538 12. Tunstead, C., et al., *The ARDS microenvironment enhances MSC-induced repair via*
539 *VEGF in experimental acute lung inflammation.* Mol Ther, 2024. **32**(10): p. 3422-
540 3432.
541 13. Boland, L., et al., *IFN-γ and TNF-α Pre-licensing Protects Mesenchymal Stromal*
542 *Cells from the Pro-inflammatory Effects of Palmitate.* Mol Ther, 2018. **26**(3): p. 860-
543 873.
544 14. Tunstead, C., Bitterlich, L.B.*, Ankrum, J.A., Hogand, A.E. and English, K.,
545 *Palmitate enhances MSC immunomodulation of human macrophages via the*
546 *ceramide/CCL2 axis in vitro.* Stem Cell Research and Therapy, 2025. 16(435).

547 15. Liu, Y., et al., *The Role of PPAR-δ in Metabolism, Inflammation, and Cancer: Many*
548 *Characters of a Critical Transcription Factor.* Int J Mol Sci, 2018. **19**(11).
549 16. Kota, B.P., T.H. Huang, and B.D. Roufogalis, *An overview on biological mechanisms*
550 *of PPARs.* Pharmacol Res, 2005. **51**(2): p. 85-94.
551 17. Lim, J. and E.K. Park, *Effect of fibroblast growth factor-2 and retinoic acid on*
552 *lineage commitment of bone marrow mesenchymal stem cells.* Tissue Eng Regen
553 Med, 2016. **13**(1): p. 47-56.
554 18. Park, J.R., et al., *Effects of Peroxisome Proliferator-Activated Receptor-δ Agonist on*
555 *Cardiac Healing after Myocardial Infarction.* PLoS One, 2016. **11**(2): p. e0148510.
556 19. Carty, F., et al., *IFN-γ and PPARδ influence the efficacy and retention of multipotent*
557 *adult progenitor cells in graft vs host disease.* Stem Cells Transl Med, 2021. **10**(11):
558 p. 1561-1574.
559 20. Heck, B.E., et al., *PPAR-δ Agonist With Mesenchymal Stem Cells Induces Type II*
560 *Collagen-Producing Chondrocytes in Human Arthritic Synovial Fluid.* Cell
561 Transplant, 2017. **26**(8): p. 1405-1417.
562 21. Luz-Crawford, P., et al., *PPARβ/δ directs the therapeutic potential of mesenchymal*
563 *stem cells in arthritis.* Ann Rheum Dis, 2016. **75**(12): p. 2166-2174.
564 22. Contreras-Lopez, R.A., Elizondo-Vega, R., Torres, M.J. *et al*, *PPARβ/δ-dependent*
565 *MSC metabolism determines their immunoregulatory properties.* 2020: p. 11423
566 23. Kim, D.H., et al., *PPAR-δ agonist affects adipo-chondrogenic differentiation of*
567 *human mesenchymal stem cells through the expression of PPAR-γ.* Regen Ther, 2020.
568 **15**: p. 103-111.
569 24. Nernpermpisooth, N., et al., *PPARβ/δ Is Required for Mesenchymal Stem Cell*
570 *Cardioprotective Effects Independently of Their Anti-inflammatory Properties in*
571 *Myocardial Ischemia-Reperfusion Injury.* Front Cardiovasc Med, 2021. **8**: p. 681002.

572 25. Sarre, C., et al., *PPARβ/δ priming enhances the anti-apoptotic and therapeutic*
573 *properties of mesenchymal stromal cells in myocardial ischemia-reperfusion injury.*
574 Stem Cell Res Ther, 2022. **13**(1): p. 167.
575 26. Djouad, F., et al., *PPARβ/δ: A master regulator of mesenchymal stem cell functions.*
576 Biochimie, 2017. **136**: p. 55-58.
577 27. Ziveri, J., et al., *Angiopoietin-like 4 protects against endothelial dysfunction during*
578 *bacterial sepsis.* Nat Microbiol, 2024. **9**(9): p. 2434-2447.
579 28. Goh, Y.Y., et al., *Angiopoietin-like 4 interacts with integrins beta1 and beta5 to*
580 *modulate keratinocyte migration.* Am J Pathol, 2010. **177**(6): p. 2791-803.
581 29. Zhan, W., et al., *ANGPTL4 attenuates palmitic acid-induced endothelial cell injury by*
582 *increasing autophagy.* Cell Signal, 2022. **98**: p. 110410.
583 30. An, Q., et al., *In vitro effects of mitomycin C on the proliferation of the non-small-cell*
584 *lung cancer line A549.* Int J Clin Exp Med, 2015. **8**(11): p. 20516-23.
585 31. Neubauer, E., et al., *Comparative evaluation of three proliferation markers, Ki-67,*
586 *TOP2A, and RacGAP1, in bronchopulmonary neuroendocrine neoplasms: Issues and*
587 *prospects.* Oncotarget, 2016. **7**(27): p. 41959-41973.
588 32. Huang, W., et al., *ANGPTL4 induces Kupffer cell M2 polarization to mitigate acute*
589 *rejection in liver transplantation.* Sci Rep, 2025. **15**(1): p. 986.
590 33. Batista, F.A., et al., *Structural insights into human peroxisome proliferator activated*
591 *receptor delta (PPAR-delta) selective ligand binding.* PLoS One, 2012. **7**(5): p.
592 e33643.
593 34. Kornicka, K., J. Houston, and K. Marycz, *Dysfunction of Mesenchymal Stem Cells*
594 *Isolated from Metabolic Syndrome and Type 2 Diabetic Patients as Result of*
595 *Oxidative Stress and Autophagy may Limit Their Potential Therapeutic Use.* Stem
596 Cell Rev Rep, 2018. **14**(3): p. 337-345.

597 35. Lu, P., et al., *Serum Free Fatty Acid Concentration Predicts ARDS after Off-Pump*
598 *CABG: A Prospective Observational Study.* Lung, 2024. **202**(5): p. 523-532.
599 36. Boland, L., et al., *Translating MSC Therapy in the Age of Obesity.* Front Immunol,
600 2022. **13**: p. 943333.
601 37. Grygiel-Górniak, B., *Peroxisome proliferator-activated receptors and their ligands:*
602 *nutritional and clinical implications--a review.* Nutr J, 2014. **13**: p. 17.
603 38. Mirza, A.Z., I.I. Althagafi, and H. Shamshad, *Role of PPAR receptor in different*
604 *diseases and their ligands: Physiological importance and clinical implications.* Eur J
605 Med Chem, 2019. **166**: p. 502-513.
606 39. Capelli, D., et al., *Structural basis for PPAR partial or full activation revealed by a*
607 *novel ligand binding mode.* Sci Rep, 2016. **6**: p. 34792.
608 40. Yang, Y., et al., *Synergism of MSC-secreted HGF and VEGF in stabilising*
609 *endothelial barrier function upon lipopolysaccharide stimulation via the Rac1*
610 *pathway.* Stem Cell Res Ther, 2015. **6**: p. 250.
611 41. Zisa, D., et al., *Vascular endothelial growth factor (VEGF) as a key therapeutic*
612 *trophic factor in bone marrow mesenchymal stem cell-mediated cardiac repair.*
613 Biochem Biophys Res Commun, 2009. **390**(3): p. 834-8.
614 42. Yang, Y., et al., *The Vascular Endothelial Growth Factors-Expressing Character of*
615 *Mesenchymal Stem Cells Plays a Positive Role in Treatment of Acute Lung Injury In*
616 *Vivo.* Mediators Inflamm, 2016. **2016**: p. 2347938.
617 43. Dunbar, H., et al., *The VEGF-Mediated Cytoprotective Ability of MIF-Licensed*
618 *Mesenchymal Stromal Cells in House Dust Mite-Induced Epithelial Damage.* Eur J
619 Immunol, 2025. **55**(1): p. e202451205.

620 44. Cahill, E.F., et al., *Hepatocyte Growth Factor Is Required for Mesenchymal Stromal*
621 *Cell Protection Against Bleomycin-Induced Pulmonary Fibrosis.* Stem Cells Transl
622 Med, 2016. **5**(10): p. 1307-1318.
623 45. Kennelly, H., B.P. Mahon, and K. English, *Human mesenchymal stromal cells exert*
624 *HGF dependent cytoprotective effects in a human relevant pre-clinical model of*
625 *COPD.* Sci Rep, 2016. **6**: p. 38207.
626 46. Cho, D.I., et al., *Antiinflammatory activity of ANGPTL4 facilitates macrophage*
627 *polarization to induce cardiac repair.* JCI Insight, 2019. **4**(16).
628 47. Curley, G.F., et al., *Effects of intratracheal mesenchymal stromal cell therapy during*
629 *recovery and resolution after ventilator-induced lung injury.* Anesthesiology, 2013.
630 **118**(4): p. 924-32.
631

632 **Figure Legends**

633 **Figure 1: Secretome from PPARβ/δ agonised hBM-MSCs enhanced wound healing in**
634 **CALU-3 lung epithelial cells.** (A) Experimental Design. A CALU-3 scratch assay was run, in
635 combination with MSC-CM from naive, PPARβ/**δ** agonized (+) or antagonized (-) hBM-
636 MSCs. (B) Images of the wound healing assay at baseline or following 48hrs fixed and stained
637 with crystal violet dye and (C) quantified using ImageJ software (one-way ANOVA followed
638 by Tukey's post-hoc test, n=3). White bar is CALU-3 cells in media alone. (D) Percentage (%)
639 wound healing in scratched CALU-3 cells was recorded at different time points (6, 24 and
640 48hrs). Mitomycin C (MMC, denoted as circular data points) was added to CALU-3 cells 2hr
641 prior to the scratch assay. Conditioned medium from naive, PPARβ/**δ** agonized (+) or
642 antagonized (-) hBM-MSCs was added immediately after the scratch. Wound closure (%) was
643 quantified using imageJ software (two-way ANOVA followed by Tukey's post-hoc test, n=3).
644 (E) Expression of the cell proliferation gene *TOP2A* was analysed by RT-PCR at a 48hr time-

645 point (one-way ANOVA followed by Tukey's post-hoc test, n=3). Replicates are a
646 representation of 3 individual hBM-MSC donors. Data is presented as mean ± SEM; *p<0.05,
647 **p<0.01, ***p<0.001, ****p<0.0001.
648
649 **Figure 2: RNA-Seq identified enrichment of ANGPTL4 in PPARβ/δ agonised hBM-**
650 **MSCs.** (A) Experimental design: hBM-MSCs exposed to 1uM of PPARβ/**δ** agonist or
651 antagonist were sent to Novogene™ for RNA sequencing. (B) Venn diagrams showing the
652 number of differentially expressed genes (DEGs) in naive, PPARβ/**δ** agonized (+) or
653 antagonized (-) hBM-MSCs. (C) Volcano plots generated using Flourish™ software highlight
654 the most significant DEGs Log10(p-value). Fragments per kilobase of transcript per million
655 mapped reads (FPKM) was plotted for two known PPARβ/**δ** target genes in the sequencing
656 dataset: (D) *ANGPTL4* and (E) *PDK4*. Expression of *ANGPTL4* (F) and *PDK4* (G) in hBM-
657 MSCs exposed to 1uM of PPARβ/**δ** agonist or antagonist for 6hrs was confirmed by real-time
658 RT-PCR (one-way ANOVA followed by Tukey's post-hoc test, n=3). Replicates are a
659 representation of 3 individual hBM-MSC donors. Data is presented as mean ± SEM; **p<0.01,
660 ***p<0.001, ****p<0.0001.
661
662 **Figure 3: PPARβ/δ(+) hBM-MSCs show enhanced expression of ANGPTL4, but not**
663 **other traditional MSC-associated genes or proteins.** Supernatant from hBM-MSCs exposed
664 to 1uM of PPARβ/**δ** agonist or antagonist were harvested before cells were collected in TRIzol
665 for gene expression studies. Protein expression of (A) ANGPTL4, (B) VEGF and (C) MIF
666 were assessed by ELISA. Gene expression of (D) *PTGS2,* (E) *IL-6,* (F) *IDO,* (G) *PTGES* and
667 (H) *TGFβ* were assessed by real-time RT-PCR (one-way ANOVA followed by Tukey's post-
668 hoc test, n=3). Replicates are a representation of 3 individual hBM-MSC donors. Data is
669 presented as mean ± SEM; *p<0.05.

670

671 **Figure 4: The secretome from PPARβ/δ agonised hBM-MSCs mediates enhanced wound**
672 **repair via ANGPTL4.** (A) Experimental design. Using an ANGPTL4 neutralisation approach,
673 we assessed wound closure of CALU-3 lung epithelial cells. (B) Images taken at baseline or
674 48hr post scratch. Scratched CALU-3 cells were incubated with isotype control or anti-
675 ANGPTL4 antibody before addition of conditioned medium. Medium only served as the
676 control. (C) % wound closure quantified using ImageJ. (D) Levels of ANGPTL4 produced by
677 naive hBM-MSCs or exposed to 1uM of PPARβ/**δ** agonist or antagonist in the presence of the
678 isotype control of anti-ANGPTL4 antibody were measured by ELISA (one-way ANOVA
679 followed by Tukey's post-hoc test, n=3). Replicates are a representation of 3 individual hBM-
680 MSC donors. ND denotes not detected. Data is presented as mean ± SEM; **p<0.01,
681 ***p<0.001, ****p<0.0001.

682

683 **Figure 5: ARDS patients have higher levels of PPARβ/δ ligands and co-activators.** (A) A
684 publicly available dataset (Study ID: ST000042; doi: 10.21228/M8SG64) was mined for
685 PPARβ/**δ** ligands present in the ARDS lung. Levels of Arachidonate, Palmitoleic acid and
686 Linoleate were elevated in ARDS bronchoalveolar lavage fluid compared to healthy controls.
687 (B) An additional RNA-Seq dataset (GEO accession no.: GSE185263), based on ARDS serum,
688 highlighted an increase in PPARβ/**δ**-associated co-activators in both SARS-CoV-2 ARDS and
689 Classical ARDS patient serum compared to Non-ARDS controls. RNA-Seq data counts for
690 PPARβ/**δ**-associated co-activator genes (C) *PPARGC1A*, (D) *NCOA1*, (E) *NCOA2*, (F)
691 *NCOA3* and (G) *CREBBP;* and co-repressor genes (H) *SIRT1*, (I) *NCOR1* and (J) *NCOR2* were
692 plotted comparing expression between SARS-CoV-2 ARDS, Classical ARDS and Non-ARDS
693 controls (one-way ANOVA followed by Tukey's post-hoc test, n=6-58). Each data point (A-J)
694 is from an individual ARDS patient, or healthy control. (K) ANGPTL4 production from 3

695 individual hBM-MSC donors exposed to PPARβ/**δ** agonist (+) or antagonist (-) in the presence
696 or absence of 20% ARDS patient serum was measured by ELISA. Data is presented as mean
697 ± SEM; *p<0.05, **p<0.01, ***p<0.001, ****p<0.0001.
698
699 **Figure 6: MSC-CM$_{PPARβ/δ(+)}$ supports enhanced endothelial barrier function in ALI.** Mice
700 were exposed to 2mg/kg LPS IT, or PBS control. Some groups received MSC-CM$_{PPARβ/δ(-)}$ or
701 MSC-CM$_{PPARβ/δ(+)}$ + isotype control or MSC-CM$_{PPARβ/δ(+)}$ + anti-ANGPTL4. (A) Lungs were
702 harvested and imaged after Evan's Blue Dye administration highlighting increased vascular
703 permeability (visible blue dye). (B) Quantification of the amount of Evan's Blue dye leakage
704 from the lungs of mice exposed to LPS +/- treatments of interest (n=5/group, or n=3 for PBS
705 control group). Levels of pro-inflammatory cytokines in the bronchoalveolar lavage fluid (C)
706 TNFα and (D) IL-6 were assessed by ELISA (one-way ANOVA followed by Tukey's post-
707 hoc test, n=4-6/group). (E) % weigh loss and (F) Clinical scores (n=4-6/group) were recorded
708 over the course of the model. Data points are a representation of individual mice. Data is
709 presented as mean ± SEM; *p<0.05, **p<0.01.
710
711 **Figure 7: ARDS-licensed MSC-CM$_{PPARβ/δ(+)}$ provide protection in ALI via ANGPTL4.**
712 Mice were exposed to 2mg/kg LPS IT, or PBS control. Some groups received ARDS licensed
713 MSC-CM$_{PPARβ/δ(+)}$ + isotype control or ARDS-licensed MSC-CM$_{PPARβ/δ(+)}$ + anti-ANGPTL4.
714 Levels of bronchoalveolar lavage fluid pro-inflammatory cytokines (A) TNFα and (B) IL-6
715 were assessed by ELISA (one-way ANOVA followed by Tukey's post-hoc test, n=3-6/group).
716 (C) % weigh loss and (D) Clinical scores (n=3-6/group) were recorded over the course of the
717 model. Data points represent individual mice. Data is presented as mean ± SEM; *p<0.05,
718 ***p<0.001.
719

Graphical Abstract

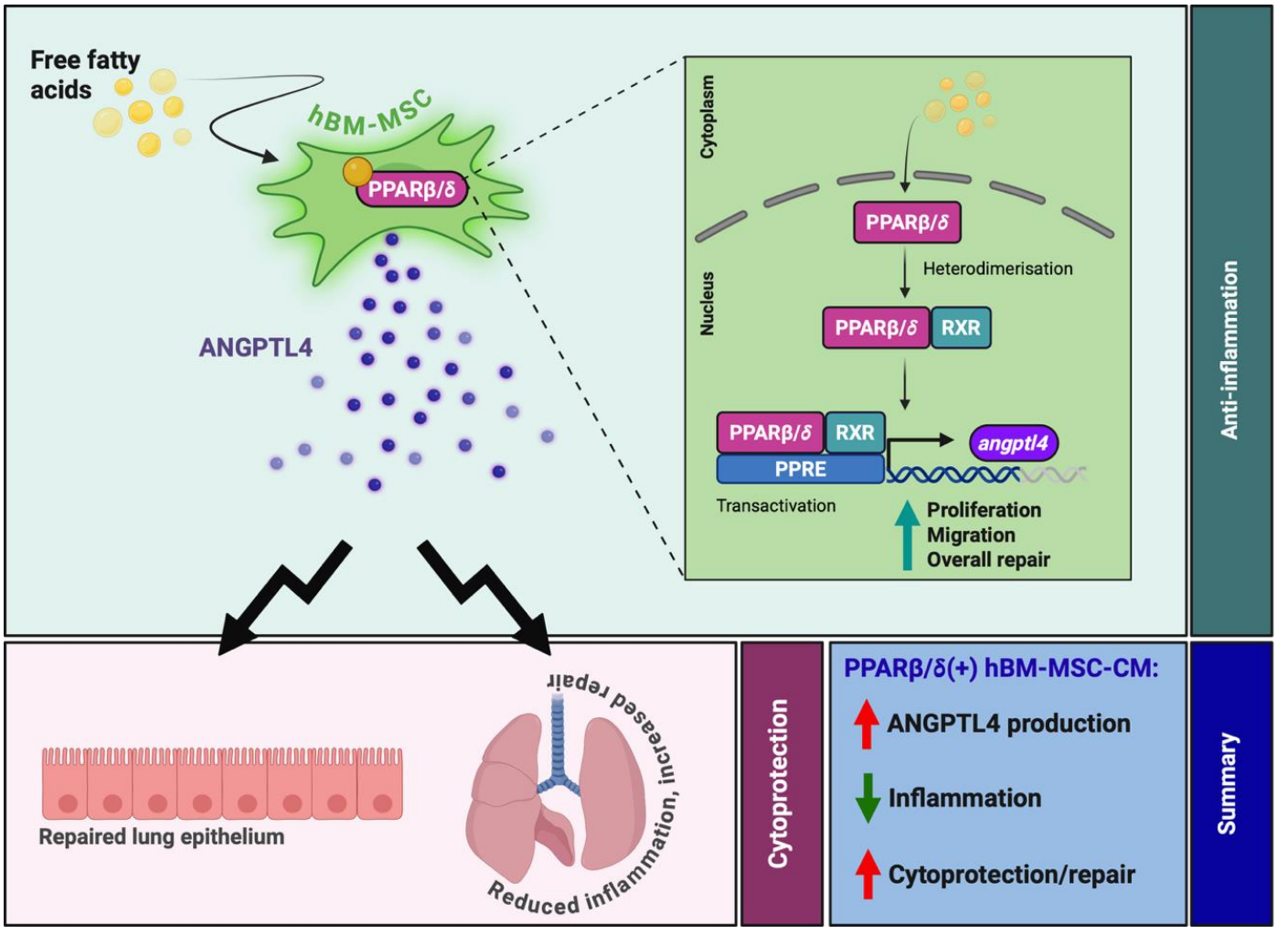

A

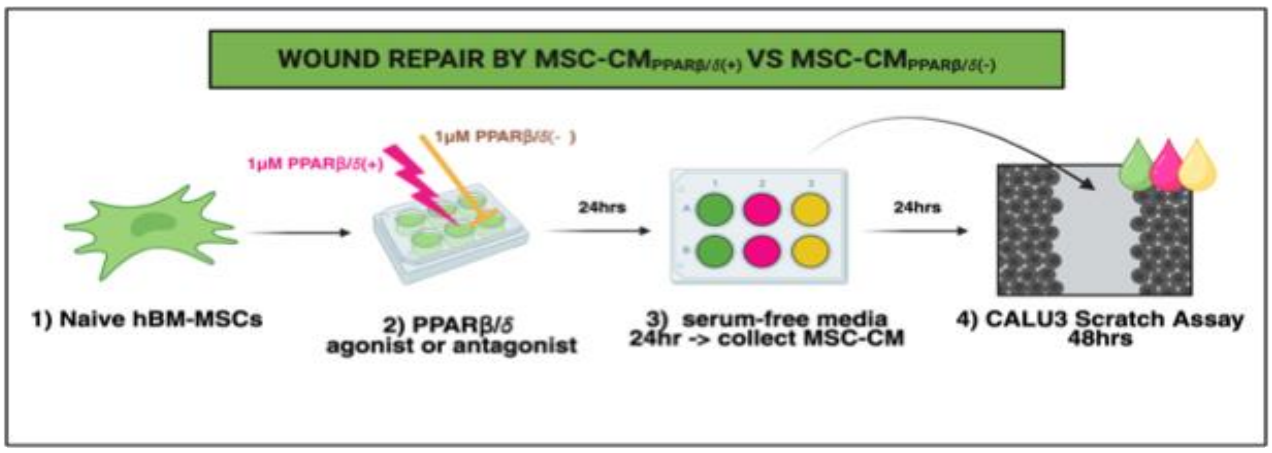

B

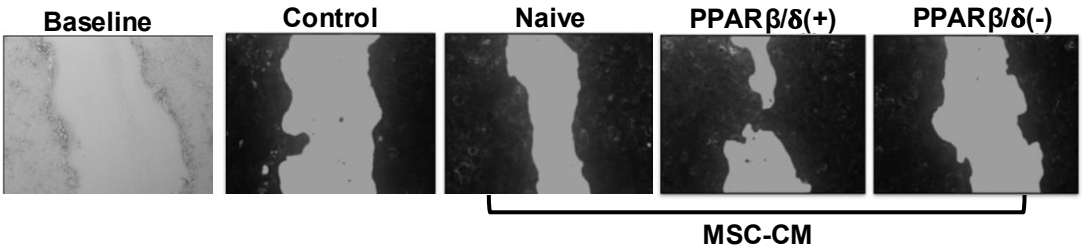

C

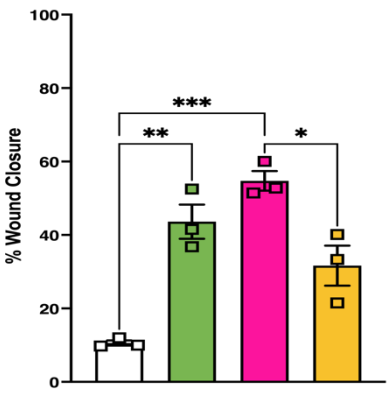

E

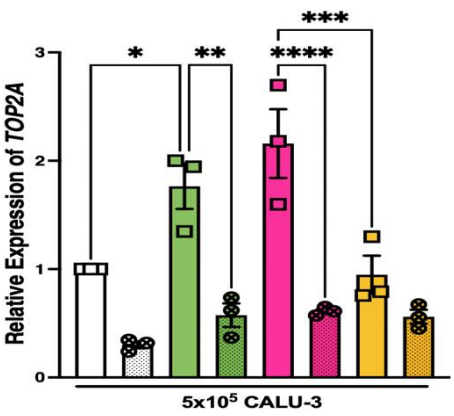

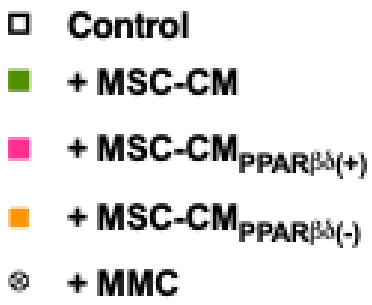

D

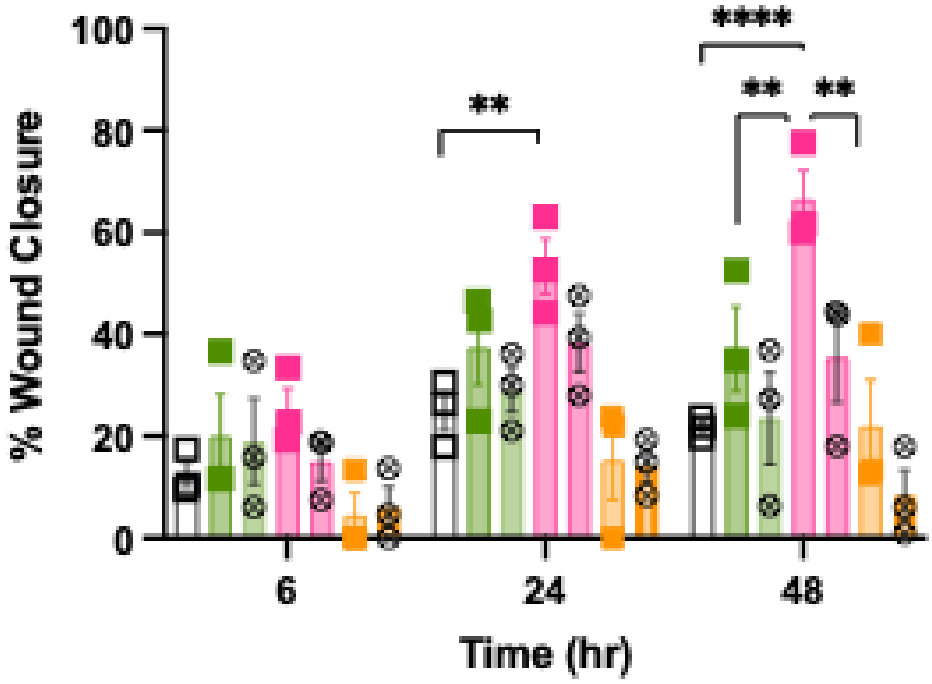

Figure 1

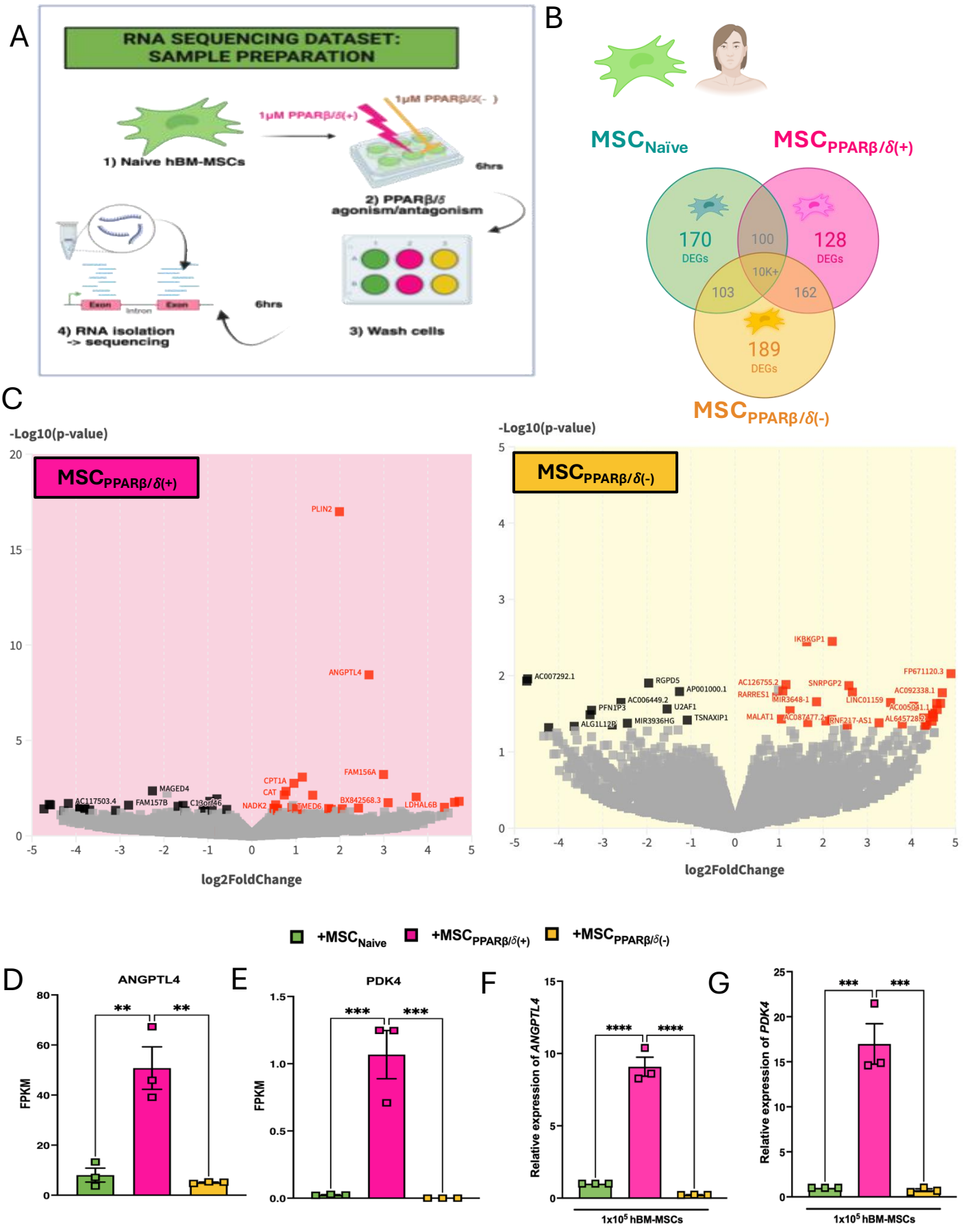
A
RNA SEQUENCING DATASET: SAMPLE PREPARATION
1) Naive hBM-MSCs
1μM PPARβ/δ(+)
1μM PPARβ/δ(-)
6hrs
2) PPARβ/δ agonism/antagonism
3) Wash cells
6hrs
4) RNA isolation -> sequencing
B
MSCNaïve
MSCPPARβ/δ(+)
MSCPPARβ/δ(-)
170 DEGs
100
128 DEGs
10K+
103
162
189 DEGs
C
-Log10(p-value)
MSCPPARβ/δ(+)
PLIN2
ANGPTL4
FAM156A
CPT1A
CAT
MAGED4
AC117503.4
FAM157B
C13orf46
NADK2
TMED6
BX842568.3
LDHAL6B
log2FoldChange
-Log10(p-value)
MSCPPARβ/δ(-)
IKBKGP1
AC007292.1
RGPD5
AP001000.1
AC006449.2
PFN1P3
U2AF1
ALG1L12P
MIR3936HG
TSNAXIP1
AC126755.2
RARRES1
MIR3648-1
SNRPGP2
LINC01159
FP671120.3
AC092338.1
MALAT1
AC087477.2
RNF217-AS1
AL645728.2
log2FoldChange
+MSCNaive
+MSCPPARβ/δ(+)
+MSCPPARβ/δ(-)
D
ANGPTL4
FPKM
E
PDK4
FPKM
F
Relative expression of ANGPTL4
1x10⁵ hBM-MSCs
G
Relative expression of PDK4
1x10⁵ hBM-MSCs

Figure 2

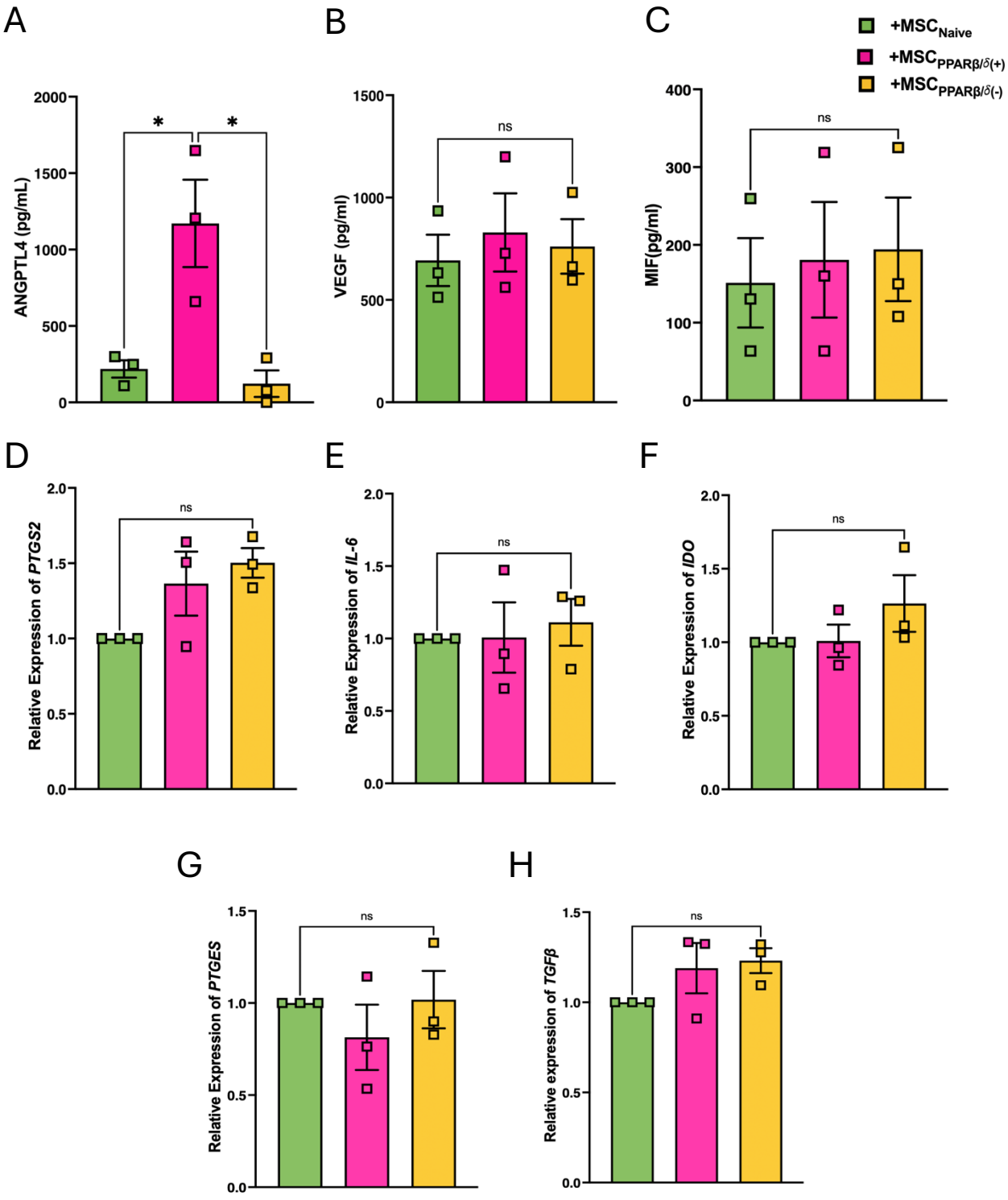
A
B
C
+MSC$_{Naive}$
+MSC$_{PPARβ/δ(+)}$
+MSC$_{PPARβ/δ(-)}$
ANGPTL4 (pg/mL)
VEGF (pg/ml)
MIF(pg/ml)
ns
D
E
F
Relative Expression of PTGS2
Relative Expression of IL-6
Relative Expression of IDO
G
H
Relative Expression of PTGES
Relative expression of TGFβ

Figure 3

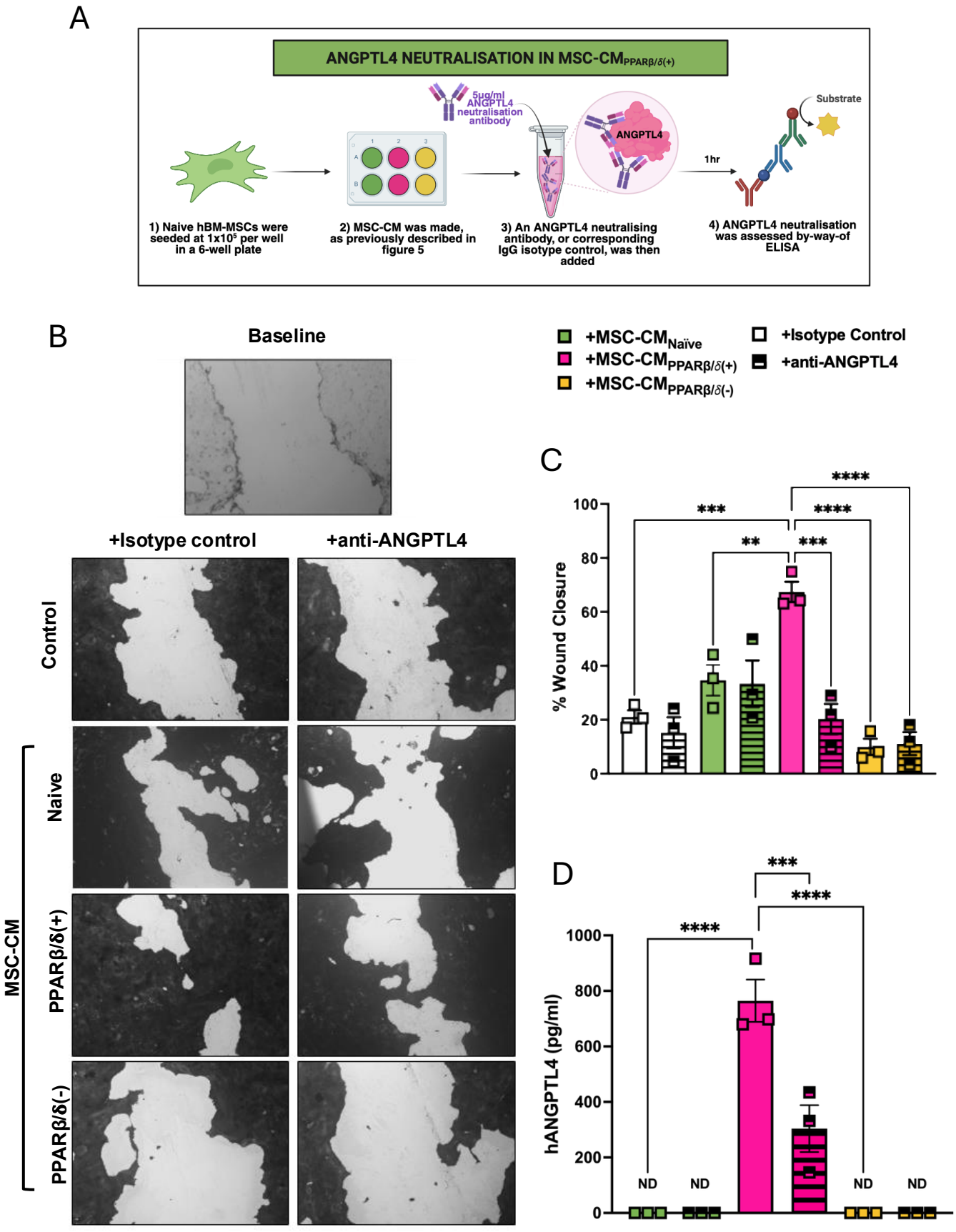
A
ANGPTL4 NEUTRALISATION IN MSC-CM$_{PPARβ/δ(+)}$
5µg/ml ANGPTL4 neutralisation antibody
ANGPTL4
1hr
Substrate
1) Naive hBM-MSCs were seeded at 1x10^5 per well in a 6-well plate
2) MSC-CM was made, as previously described in figure 5
3) An ANGPTL4 neutralising antibody, or corresponding IgG isotype control, was then added
4) ANGPTL4 neutralisation was assessed by-way-of ELISA
B
Baseline
+Isotype control
+anti-ANGPTL4
Control
Naive
PPARβ/δ(+)
PPARβ/δ(-)
MSC-CM
+MSC-CM$_{Naïve}$
+MSC-CM$_{PPARβ/δ(+)}$
+MSC-CM$_{PPARβ/δ(-)}$
+Isotype Control
+anti-ANGPTL4
C
% Wound Closure
100
80
60
40
20
0
***
****
**
***
****
D
hANGPTL4 (pg/ml)
1000
800
600
400
200
0
***
****
****
ND
ND
ND
ND

Figure 4

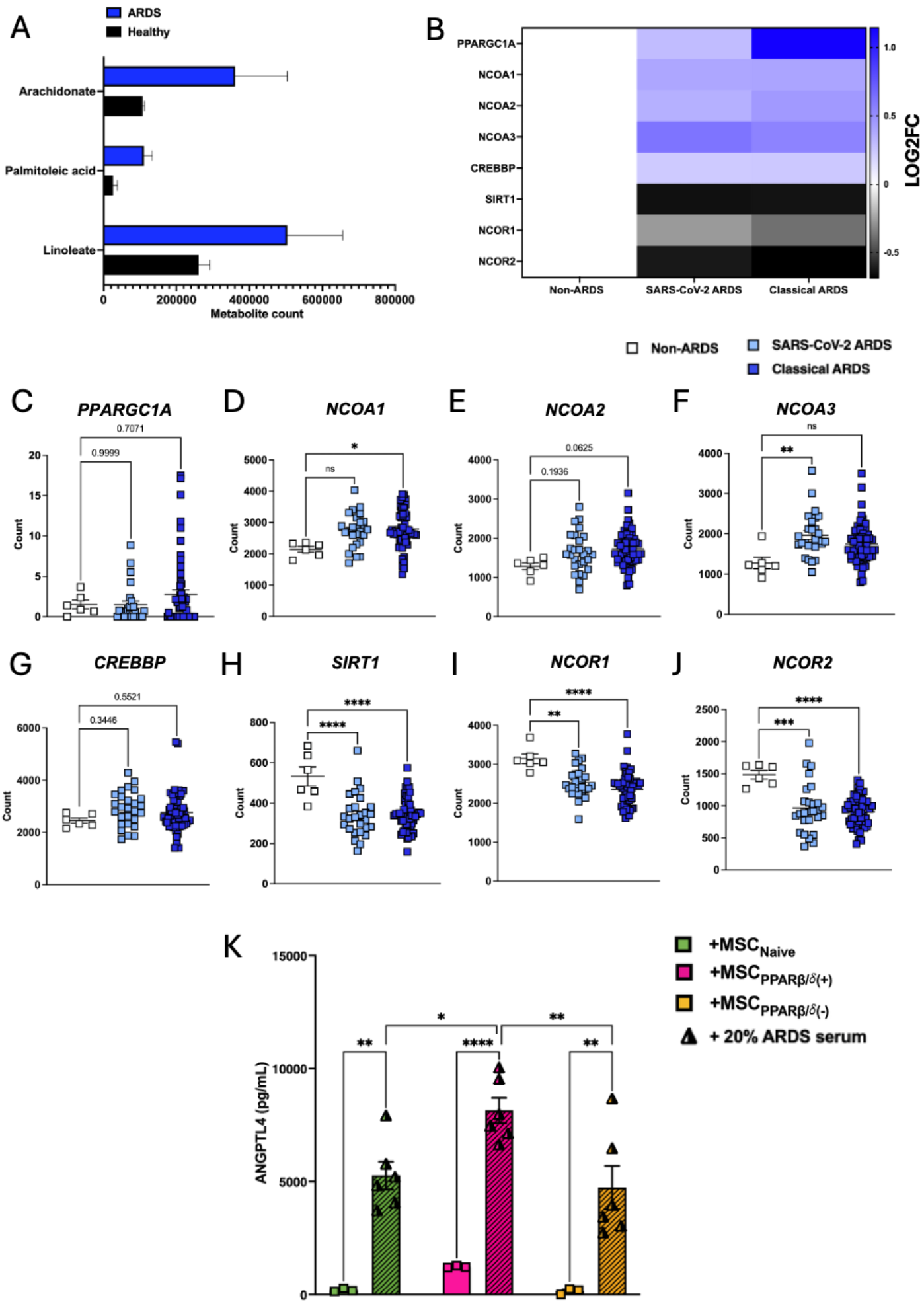
A
ARDS
Healthy
Arachidonate
Palmitoleic acid
Linoleate
0
200000
400000
600000
800000
Metabolite count
B
PPARGC1A
NCOA1
NCOA2
NCOA3
CREBBP
SIRT1
NCOR1
NCOR2
Non-ARDS
SARS-CoV-2 ARDS
Classical ARDS
LOG2FC
1.0
0.5
0
-0.5
Non-ARDS
SARS-CoV-2 ARDS
Classical ARDS
C
PPARGC1A
0.7071
0.9999
Count
D
NCOA1
*
ns
E
NCOA2
0.0625
0.1936
F
NCOA3
ns
**
G
CREBBP
0.5521
0.3446
H
SIRT1
****
****
I
NCOR1
****
**
J
NCOR2
****
***
K
ANGPTL4 (pg/mL)
15000
10000
5000
0
*
**
**
****
**
+MSC$_{Naive}$
+MSC$_{PPARβ/δ(+)}$
+MSC$_{PPARβ/δ(-)}$
+ 20% ARDS serum

Figure 5

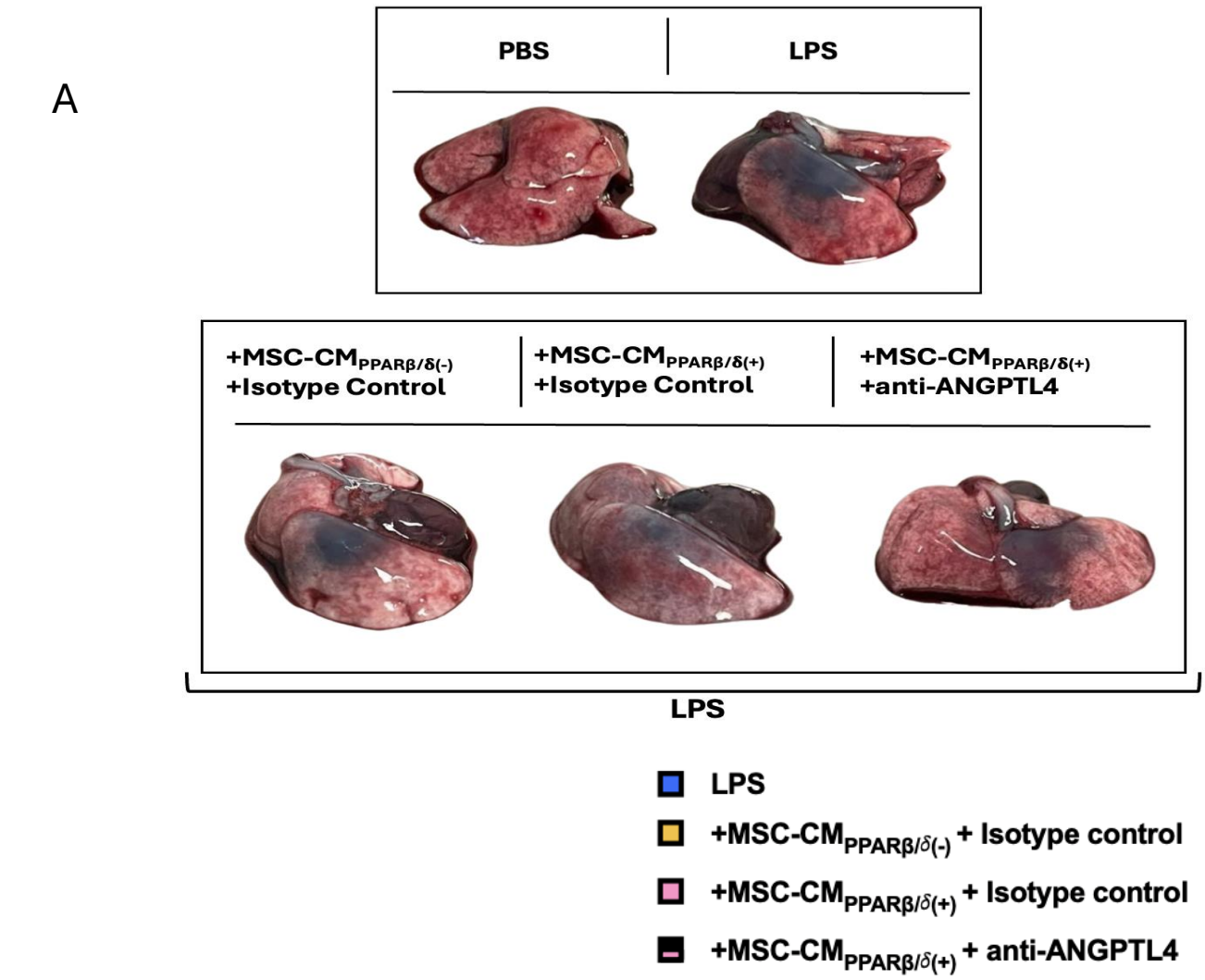
A
PBS
LPS
+MSC-CM$_{PPARβ/δ(-)}$
+Isotype Control
+MSC-CM$_{PPARβ/δ(+)}$
+Isotype Control
+MSC-CM$_{PPARβ/δ(+)}$
+anti-ANGPTL4
LPS
LPS
+MSC-CM$_{PPARβ/δ(-)}$ + Isotype control
+MSC-CM$_{PPARβ/δ(+)}$ + Isotype control
+MSC-CM$_{PPARβ/δ(+)}$ + anti-ANGPTL4

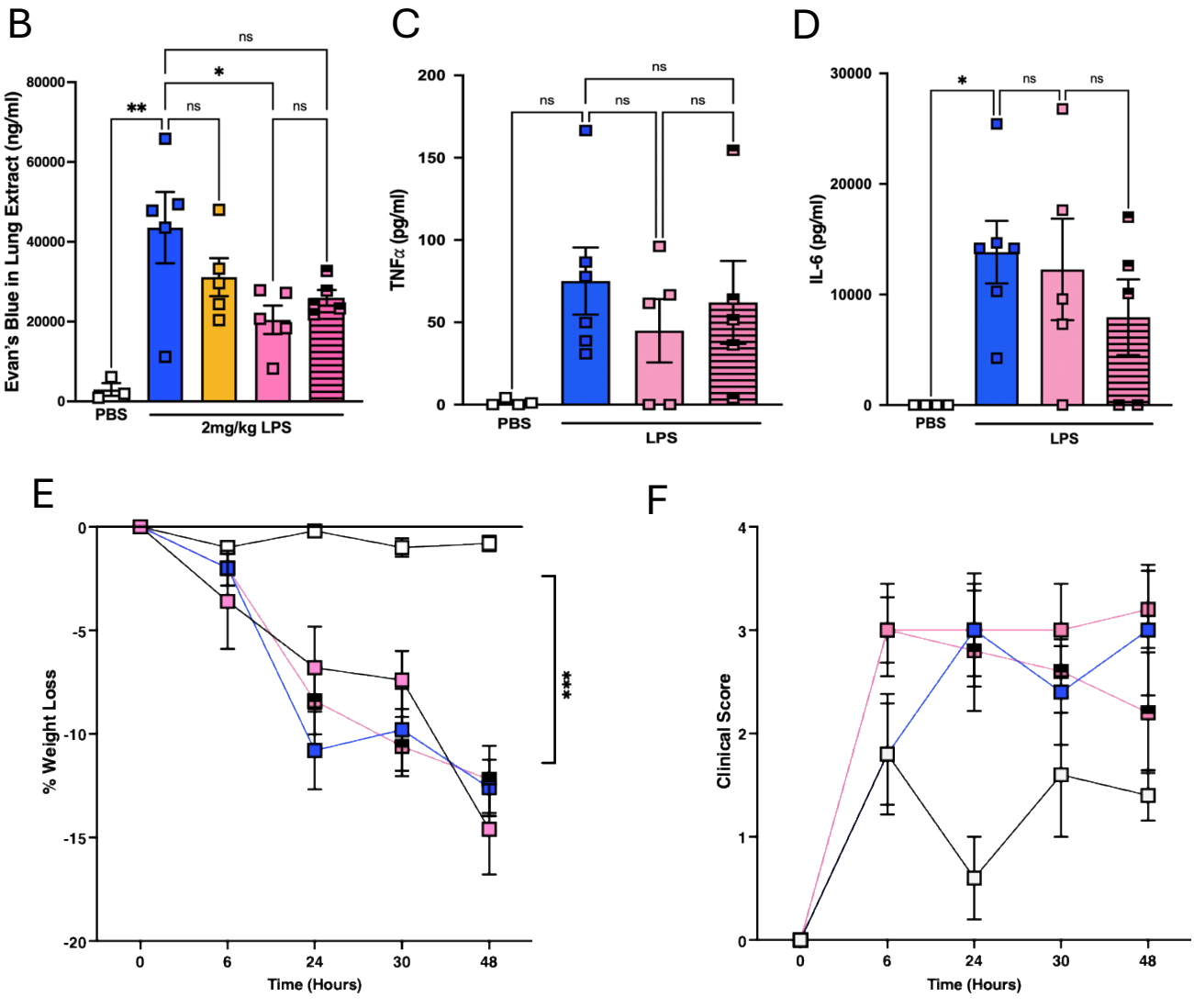
B
Evan's Blue in Lung Extract (ng/ml)
80000
60000
40000
20000
0
**
*
ns
ns
ns
PBS
2mg/kg LPS
C
TNFα (pg/ml)
200
150
100
50
0
ns
ns
ns
ns
PBS
LPS
D
IL-6 (pg/ml)
30000
20000
10000
0
*
ns
ns
PBS
LPS
E
% Weight Loss
0
-5
-10
-15
-20
***
0
6
24
30
48
Time (Hours)
F
Clinical Score
4
3
2
1
0
0
6
24
30
48
Time (Hours)

Figure 6

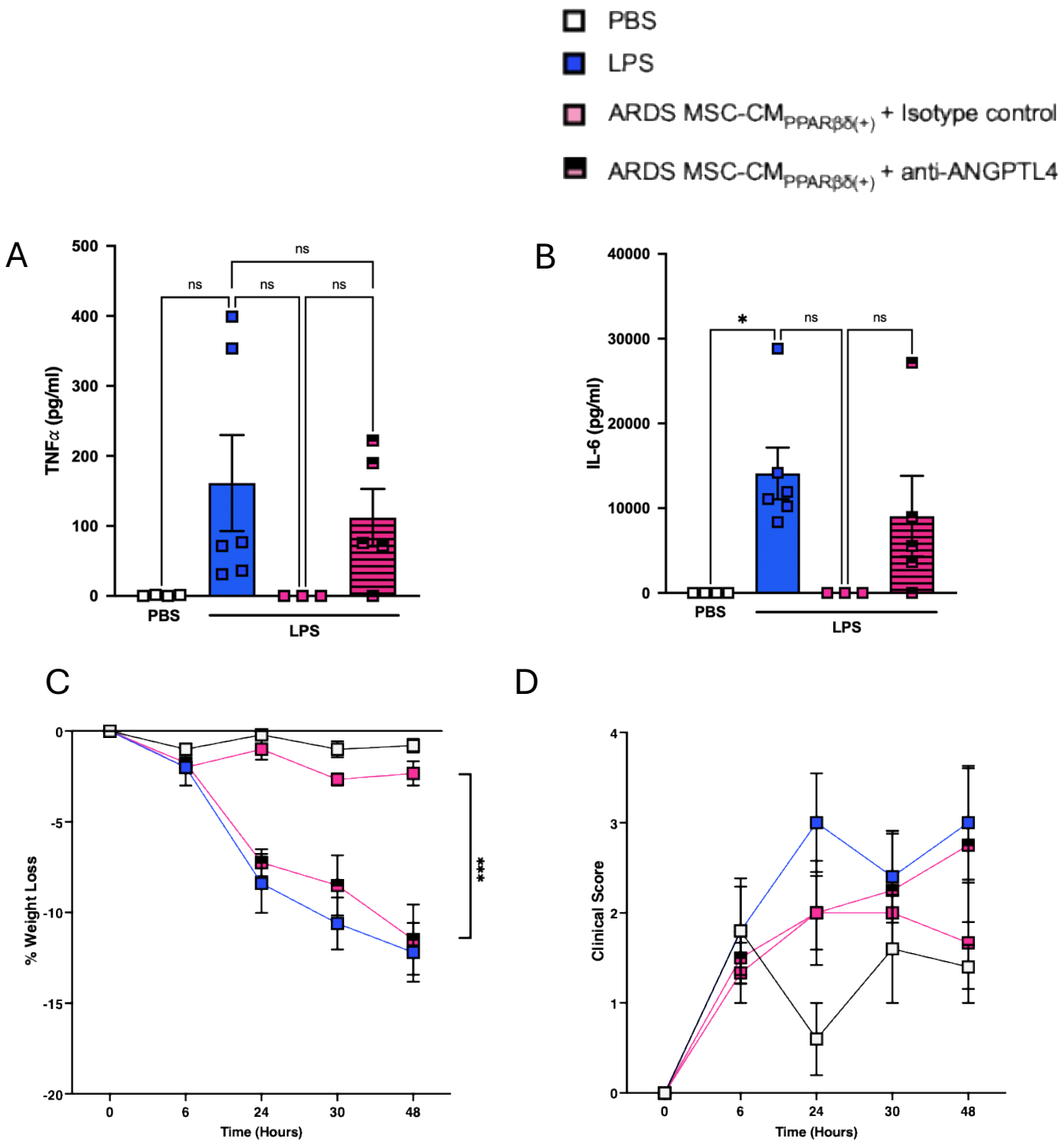
PBS
LPS
ARDS MSC-CM$_{PPARβδ(+)}$ + Isotype control
ARDS MSC-CM$_{PPARβδ(+)}$ + anti-ANGPTL4
A
TNFα (pg/ml)
500
400
300
200
100
0
ns
ns
ns
ns
PBS
LPS
B
IL-6 (pg/ml)
40000
30000
20000
10000
0
*
ns
ns
PBS
LPS
C
% Weight Loss
0
-5
-10
-15
-20
***
0
6
24
30
48
Time (Hours)
D
Clinical Score
4
3
2
1
0
0
6
24
30
48
Time (Hours)

Figure 7